Made available through a Creative Commons CC-BY License

NANO LETTERS

ACS AUTHORCHOICE

pubs.acs.org/NanoLett

Letter

# Kinetics of Toehold-Mediated DNA Strand Displacement Depend on $Fe^{II}_4L_4$ Tetrahedron Concentration

Jinbo Zhu, Filip Bošković, Bao-Nguyen T. Nguyen, Jonathan R. Nitschke,* and Ulrich F. Keyser*

Cite This: *Nano Lett.* 2021, 21, 1368−1374

Read Online

ACCESS | Metrics & More | Article Recommendations | Supporting Information

**ABSTRACT:** The toehold-mediated strand displacement reaction (SDR) is a powerful enzyme-free tool for molecular manipulation, DNA computing, signal amplification, etc. However, precise modulation of SDR kinetics without changing the original design remains a significant challenge. We introduce a new means of modulating SDR kinetics using an external stimulus: a water-soluble $Fe^{II}_4L_4$ tetrahedral cage. Our results show that the presence of a flexible phosphate group and a minimum toehold segment length are essential for $Fe^{II}_4L_4$ binding to DNA. SDRs mediated by toehold ends in different lengths (3−5) were investigated as a function of cage concentration. Their reaction rates all first increased and then decreased as cage concentration increased. We infer that cage binding on the toehold end slows SDR, whereas the stabilization of intermediates that contain two overhangs accelerates SDR. The tetrahedral cage thus serves as a versatile tool for modulation of SDR kinetics.

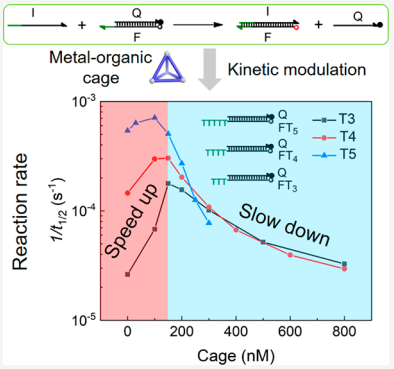


**KEYWORDS:** *metal−organic cage, DNA strand displacement, kinetics, fluorescence, molecular interaction*

DNA nanotechnology relies on the toehold-mediated strand displacement reaction (SDR). This reaction between two DNA structures initiates at the single-stranded (sticky) end, called a toehold, where the shorter strand in the duplex exchanges with a longer complementary invader strand, requiring no enzymatic mediation.[1] After having been introduced by Yurke et al. in 2000,[2] SDR has been used to transfer information in DNA computing,[3−5] to amplify signals in catalytic biosensors,[6−8] to power the movement of DNA motors and robots,[9−11] construct reprogrammable DNA nanostructures, devices, soft materials, and systems,[12−18] and even applied in living cells.[19] The reaction rates of SDR increase exponentially with toehold length, making it an easy way to tune kinetics.[20] To provide flexible control, alternative strand displacement mechanisms, such as remote toehold[21] and allosteric toehold,[22] have been developed to regulate the reaction rate, but these methods require additional spacer domains or invader strands. The presence of these additional sequences complicates the design, and precise tuning of SDR kinetics following DNA strand design is not possible using current methods. Thus, a means to precisely adjust the kinetics of toehold mediated SDR without changing the original design, DNA sequence, and structure would be of value to the community.

Over the last decades, various metal−organic cages with different three-dimensional structures have been synthesized.[23−26] Their tunable sizes and properties have enabled these cages to be used in numerous applications including catalysis,[27] separations,[28] molecule sensing,[29] and the stabilization of reactive species.[30] Recent biomedical applications of cages have attracted attention,[31] for instance in drug delivery,[32−34] cancer therapy,[35,36] and biosensing.[37] To exploit their properties relevant to these applications, cages must interact specifically with biomacromolecules. Our previous work has shown that water-soluble tetrahedral cage $Fe^{II}_4L_4$ (cage **1** in Figure 1b) binds to nonpaired bases in DNA structures.[38] Ferrous ions occupy the four vertices of this cage, and tris(4-aminophenyl)methanol residues define the four faces of the tetrahedron.[39] Cage assembly using ferrous sulfate enables preparation in aqueous buffer solution. Since free nucleotides on toehold ends and intermediates are present during SDR, we inferred that cage **1** may bind to these domains and alter the kinetics of SDR. Studies undertaken herein provided strong support for this hypothesis, indicating that the cage can regulate the kinetics of SDR in a concentration-specific manner.

We first employed the fluorescence-quenching property of the cage, as demonstrated in previous work,[38] to study the interaction between cage **1** and different DNA structures with fluorescent labels (Figure 1a). As shown in Figure 1c, the fluorescent tag fluorescein (6-FAM) on DNA duplex D1 without free nucleotides is minimally quenched in the presence

**Received:** October 15, 2020
**Revised:** December 29, 2020
**Published:** January 28, 2021

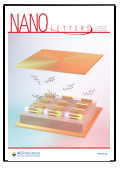

ACS Publications

© 2021 The Authors. Published by American Chemical Society



https://dx.doi.org/10.1021/acs.nanolett.0c04125
*Nano Lett.* 2021, 21, 1368−1374

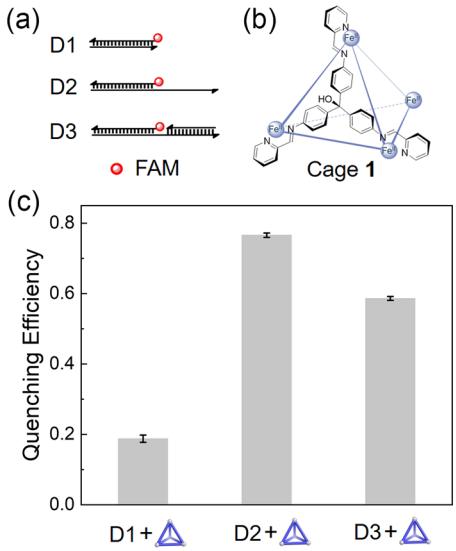


**Figure 1.** Interaction between cage **1** and different DNA structures containing fluorescence labels (fluorescein, FAM, in red). (a) DNA and (b) cage structure. (c) Quenching efficiency (QE, Supporting Information S1.5) was used to quantify the quenching effects of 0.2 $\mu$M cage **1** on each DNA structure (0.1 $\mu$M). The fluorescence intensity was measured in TSM buffer (10 mM Tris-$H_2SO_4$, 10 mM $MgSO_4$, pH 7.5). Error bars are based on three independent measurements. Information on DNA can be found in Tables S1 and S2.

of cage **1**, with a quenching efficiency (QE, Supporting Information S1.5) of only 0.19. Once free nucleotides are present to form an overhang in DNA D2, the QE increased to 0.77. This is the expected outcome because the cage binds preferentially to unpaired DNA nucleotides, as reported previously.[38] The QE for nicked DNA molecule D3 is still as high as 0.59, even though the overhang is fully hybridized with the complementary strand. This result implies that the cage bound selectively to the DNA nick. We infer that the loose base pairs and enhanced local flexibility around the DNA nick site thus provide a good site for cage binding, leading to high QE.[40] These results thus indicated that cage **1** binds selectively to unpaired nucleotides and loose base pairs.

To further understand the underlying mechanism of cage **1** binding to DNA overhangs, a series of DNA duplex molecules were prepared and treated with **1** (Figure 2a). First, we found that the length of overhang affects the quenching. This inference is supported by the data shown in Figures 2a and S1a. By comparing DT2, DT3, and DT5, which contain two, three, and five dT nucleotides, respectively, we observed greater cage quenching of fluorescence for strands having longer overhangs. Second, overhangs containing different pentanucleotides (DT5, DC5, and DA5, Figure 2a) showed similar quenching behavior. We infer thus that cage **1** binds more strongly to thymines than to adenines and cytosines, but the differences are small. Guanine was not investigated here because of its quenching effect on FAM.[41] Third, we compared the binding of cage **1** to DNA duplex molecules with different chemical structures at the extended domain (DT2, DS3, DS6, and DS9 in Figure 2b). As shown in Figures 2a and S1b, the fluorescence intensities of DS6 and DS9 are close to those observed in the case of intact duplex D1, which indicates that the contribution of the additional carbon chain to cage binding is limited. However, the presence of the flexible phosphate group (highlighted in green in Figure 2b) in the overhang of DS3 promotes the cage-based quenching and makes it approach the magnitude observed in DT2. We infer the phosphate group to enhance binding through electrostatic interactions with the positively charged cage. Although the phosphate groups also distribute along the side chains of D1, they are immobilized in the stiff double helix structure rather than in the flexible overhang. To further verify the role of the phosphate groups in cage binding, we phosphorylated the 3′ end of the nick site in D3, next to the 5′-FAM label (D3p, Figure 2c). The additional phosphate group enhanced the cage-based quenching (Figure S2) and improved the binding affinity (Figure S1c). We replaced the negatively charged

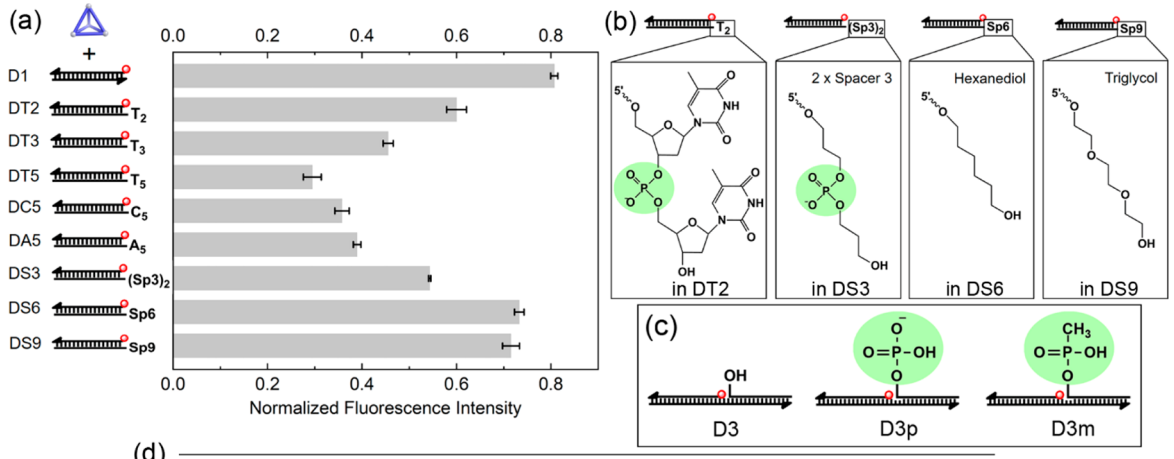


(d)

| DNA | D1 | DT5 | DT3 | DT2 | DS3 | DS6 | DS9 | D3 | D3p | D3m |
|---|---|---|---|---|---|---|---|---|---|---|
| $K_d$/μM | 1.08 | 0.186 | 0.299 | 0.340 | 0.320 | 0.575 | 0.677 | 0.247 | 0.123 | 0.278 |

**Figure 2.** Effects of the chemical structure of nonpaired DNA domains on cage **1** binding, as gauged using fluorescence quenching. (a) Bar graph of fluorescence intensities of various DNA structures (0.1 $\mu$M) with 0.2 $\mu$M cage **1** in TSM buffer. The intensity for each bar is normalized to the fluorescence intensity of the corresponding DNA structure without cage; error bars are from three independent measurements. (b, c) Chemical structures of DT2, DS3, DS6, DS9, D3, D3p, and D3m strands at specific end close to the fluorescent label. (d) Dissociation constants ($K_d$) calculated from cage titration curves in Figure S1 for different DNA structures as shown in panels a–c.


https://dx.doi.org/10.1021/acs.nanolett.0c04125
Nano Lett. 2021, 21, 1368−1374

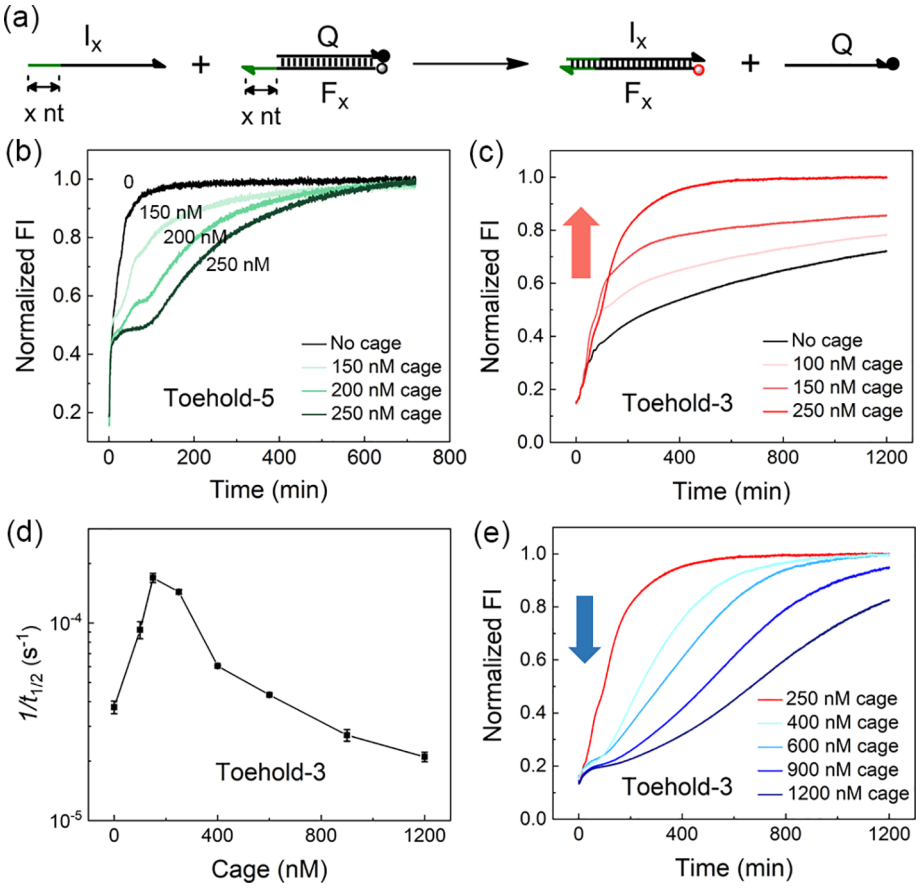


**Figure 3.** Modulation of the kinetics of toehold-5 and toehold-3 mediated strand displacement reactions by cage **1**. (a) Schematic diagram of the toehold mediated SDR; x is 5 and 3 for the toehold-5 and toehold-3 mediated strand displacements, respectively. (b) Kinetic curves showing fluorescence intensity (FI) evolution during toehold-5 mediated strand displacements with different concentrations of cage **1** in TSM buffer (5 mM $MgSO_4$). (c, e) Kinetic curves of toehold-3 mediated strand displacement with different concentrations of cage **1** in TSM buffer (10 mM $MgSO_4$). (d) Changes in the reciprocal of half completion time ($t_{1/2}$) of toehold-3 mediated SDR as a function of cage concentration. Concentrations of all DNA strands Ix, Fx, and Q are 20 nM. Cage **1** was mixed with DNA complex Fx•Q before measurement, and strand Ix was added after 1 min. The FI of the fastest group at the end of measurement is normalized to 1 in panels b, c, and e.

phosphate group by a neutral methylphosphate group (D3m, Figure 2c) and received a similar quenching result for D3 and D3m (Figure S1, S2) at similar $K_d$ (Figure 2d). However, the $K_d$ was a factor of 2 larger than for the D3p, which demonstrates the importance of the negative side-chain charge for cage binding. The dissociation constants for all our tested DNA structures are listed in a table in Figure 2d. We also investigated the effect of temperature on cage binding. As an example, we chose DT5 and measured cage interaction at elevated temperature of up to 70 °C. The results are presented in Figure S3, where the low fluorescence intensity (FI) between 15 and 30 °C indicates that cage **1** binds tightly to DNA. During the gradual increase of the temperature beyond 30 °C, the FI increases gradually until leveling off at around 60 °C. The main reason for the FI increase is due to the thermal instability of the cage, as we have shown elsewhere.[38]

Since the essential DNA structure for toehold-mediated DNA strand displacement is a DNA duplex with an overhang (Figure 3a), that is similar to the structures of DX5 (X = T, C, A) investigated in Figure 2, we hypothesized that cage **1** might bind to the unpaired overhang segment in the same way as the binding of cage **1** to DX5 and ssDNA[38] and thus influence the course of the strand displacement reaction. We first examined a DNA duplex containing a toehold end with five nucleotides (toehold-5) to study the effect of cage **1** on the SDR. As shown in Figure 3a and 3b, fluorescence of the substrate strand F (containing the fluorescent label and toehold end) is initially suppressed by the quencher appended to complementary strand Q. Following addition of invader strand I, fluorescence should thus increase. We used a buffer with a lower concentration of $Mg^{2+}$ (5 mM) in the case of toehold-5 to capture more detailed information because strand exchange initially occurred too rapidly for this strand in 10 mM $Mg^{2+}$ buffer. As shown in Figure 3b and Table S3, in the presence of cage **1**, the reaction rate slowed as the concentration of the cage increased, with all reactions having reached completion within 700 min. This result demonstrates that cage **1** influences the kinetics of SDR but it does not change the extent of reaction. In addition, if the base mismatch happened in the toehold domain, the speed of the SDR was very slow (dash lines, Figure S4). Since the cage can bind to the DNA bulge caused by base mismatch,[38] it stabilized the mismatched bases and accelerated the SDR (solid lines, Figure S4).

We next investigated the impact of cage **1** upon SDR mediated by a shorter toehold, toehold-3, containing only three nucleotides. Strand displacement is slow for toehold-3 (Figure 3c), as expected given the positive correlation between toehold length and SDR rate. However, the presence of cage **1** was observed to accelerate the rate of SDR, with a maximum rate enhancement observed with 250 nM of cage **1**. This result


https://dx.doi.org/10.1021/acs.nanolett.0c04125
Nano Lett. 2021, 21, 1368−1374

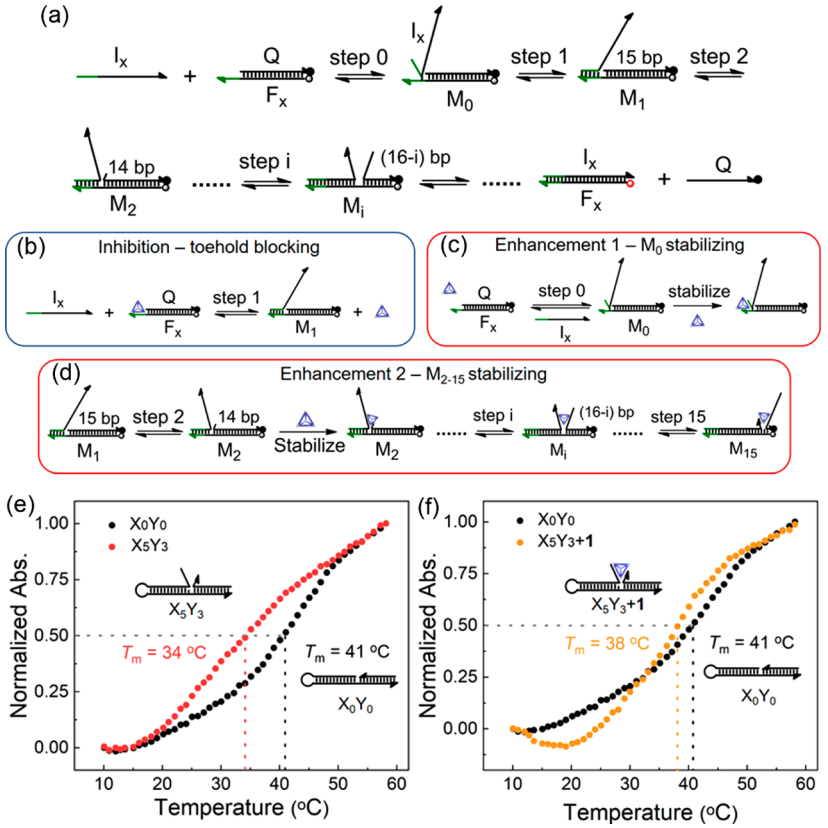


**Figure 4.** Analysis of the effects of cage **1** on the kinetics of SDR. (a) Reaction details of the toehold mediated SDR. Key reaction steps for (b) SDR inhibition and (c, d) enhancement induced by the cage are depicted. Binding of the cage onto the other nonpaired domains (such as Ix and released Q) was ignored here to simplify the analysis. (e, f) Melting curves of different DNA structures show the destabilization caused by the overhangs ($X_5Y_3$) and the stabilizing effect from the cage ($X_5Y_3$+**1**). The final curve of the mixture ($X_5Y_3$+**1**) is obtained by subtracting the melting curve of cage **1** from its original curve (Figure S7). The absorbance at 58 °C is normalized to 1.

contrasts with the situation observed in the case of toehold-5 mediated SDR.

Beyond 250 nM, cage **1** was observed to slow the rate of SDR (Figure 3e), as was observed in the case of toehold-5. As shown in Figure 3d and Table S4, the rate of toehold-3 mediated SDR, gauged by the reciprocal of half completion time, as a function of cage concentration initially rising and then falling.

To explain the concentration-dependent effect of cage **1** on the kinetics of toehold-mediated strand displacement, each step of the reaction must be considered separately. The process of toehold mediated SDR is shown schematically in Figure 4a, and its possible energy landscapes are presented in Figure S5.[42] As Ix and Q remain the same in all reactions, the only relevant difference between experiments is the number of unpaired nucleotides of the toehold on Fx. During SDR, when the cage **1** bound to Ix is removed after the hybridization of Ix and F, the released strand Q will bind to the cage at the same time. Ix has the same sequence as Q except the toehold binding domain (3−5 bases). Two FAM-labeled ssDNA differing only by three bases (FT5 and FT2, Table S1) were compared for cage binding to mimic Ix and Q. As expected, similar $K_d$ values were obtained for them and the cage showed a slightly higher affinity to the longer one (Figure S6). Therefore, cage **1** binding to Ix is tighter than to Q, and increasing the length of Ix leads to tighter binding, which explains why toehold-5 mediated SDR is inhibited at lower concentrations of cage **1** than toehold-3. For clarity in the following discussion, we will focus on the state having cage bound to the F•Q complex as cage bound to the single-stranded Ix and Q strands is the same for all systems.

Figure 4b shows our postulated mechanism for how cage **1** inhibits SDR. The toehold end in step 1 is bound to cage **1** before being invaded by strand Ix. The presence of bound cage at this key domain would increase the energy barrier for the initial binding of Ix (Figure S5a), thus slowing the reaction.

Longer unpaired overhang sequences lead to tighter cage binding (Figure 2a). Hence, the inhibitory effect is clearer in the case of toehold-5, and a higher concentration of cage is necessary to slow the reaction in cases involving the short toehold (Figure 3e).

We ascribe the acceleration of toehold-3 mediated SDR by the cage at concentrations below 250 nM (Figure 3c) to the stabilizing effect of cage **1** on the DNA intermediates $M_0$ and $M_2$−$M_{15}$ (Figure 4a), which are stepped through as strand displacement proceeds. As shown in Figure 4c, at the low concentration of cage **1**, although the short toehold end bound to the cage loosely, the intermediate $M_0$ with two overhangs at the toehold domain provided more free nucleotides to enhance the binding. At the same time, the unstable structure $M_0$ was stabilized and the initial energy barrier of SDR was reduced (Figure S5b). In intermediates $M_2$−$M_{15}$, two overhangs are also present. As reported by Winfree and co-workers,[42] the second overhang on the DNA intermediate from step 2 will cause destabilization of the DNA complex, increasing the energy barrier to SDR. This destabilization effect of the second


https://dx.doi.org/10.1021/acs.nanolett.0c04125
Nano Lett. 2021, 21, 1368−1374

overhang is also verified here in Figure 4e by comparing the melting temperatures ($T_m$) of $X_0Y_0$ and $X_5Y_3$. To mimic the condition of an F•Q•Ix DNA intermediate, the same sequence was used for the $X_iY_j$ complex except the poly-T loop and overhangs of $X_iY_j$ (Table S1), where "i" and "j" define the lengths of the overhangs on strands X and Y, respectively. The two short overhangs of $X_5Y_3$ decreased the melting temperature ($T_m$) compared to $X_0Y_0$.

Furthermore, when cage **1** was added to $X_5Y_3$, the $T_m$ increased (Figure 4f), implying that cage **1** enhanced the stability of the DNA intermediate. In the SDR, the second overhang was generated in step 2 (M2, Figure 4d), which increased the instability and incurred a free energy penalty for branch migration. The newly formed unpaired nucleotide provides an ideal binding site for the cage, however, leading **1** to bind and stabilize the DNA intermediate $M_2$, lowering the energy barrier to SDR (Figure S5b). A similar energy-lowering effect would be observed for the subsequent intermediates $M_3$−$M_{15}$. Since the inhibitory effect is weak for toehold-3 at low concentrations of cage, the accelerating effect plays a dominant role in this concentration range. Further addition of cage **1** would enhance inhibition, finally slowing the reaction. Thus, the toehold-3 mediated strand displacement rate rose first and then dropped as progressively more cage **1** was added (Figure 3d). The effect of cage **1** on the stability of dsDNA with short overhang ($Y_3$+c$Y_0$) was also investigated (Figure S8), but its $T_m$ was not substantially changed.

In principle, the two enhancement factors should also apply to toehold-5 mediated SDR, but they are counteracted by tight toehold binding, ultimately causing inhibition. However, when the concentration of cage decreased to a low enough level to weaken the initial toehold blocking, the acceleration of toehold-5 mediated SDR in low $Mg^{2+}$ buffer was also observed (Figure S9). This result supports our mechanism for the cage concentration based kinetic modulation of SDR.

To further verify the mechanism of kinetics change upon cage binding for more toehold lengths without considering sequence-dependence, we investigated the SDRs mediated by poly-T toeholds with 3−5 T nucleotides (FT3−5, Table S1) as shown in Figures 5 and S10. The reaction rates of these three kinds of toeholds all increased with **1** concentration up to a maximum value, subsequently slowing as **1** increased further. The cage concentration at the most rapid rate for each toehold increased as the toehold length decreased, which supports the conclusion that more cage is needed to slow the shorter-toehold-mediated SDR. Figure 5 summarizes the effect of cage concentration on the SDR mediated by toehold ends of different lengths, which provides guidance on modulating SDR kinetics for future applications.

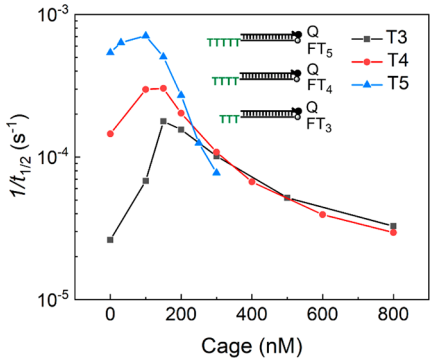


**Figure 5.** Dependence of the reciprocal of half completion time ($1/t_{1/2}$) of toehold-T3, -T4, and -T5 mediated SDRs on the cage concentration; half completion times ($t_{1/2}$) were obtained from the kinetic data in Figure S10.

In conclusion, we first studied how tetrahedral $Fe^{II}_4L_4$ cage **1** binds to unpaired nucleotides in duplex DNA. The flexible phosphate groups of single-stranded DNA provided cage binding sites. The longer the overhang, the tighter the binding of the cage to DNA, with different DNA bases affecting binding only to a limited extent. On the basis of this information, we were able to use cage **1** to modulate the kinetics of toehold-mediated DNA SDR.

The SDRs mediated by toehold ends in different lengths (3−5) were all first accelerated and then inhibited with increasing concentration of cage **1**. We infer the inhibitory effect to be caused by cage binding on the toehold end, and the acceleration to be due to stabilization of the intermediates involving the binding of the second overhang to the cage. This knowledge enables fine control over the kinetics of toehold-mediated SDR, from acceleration to deceleration, governed by tetrahedral cage **1**, thus providing a new means to tune SDR using an external stimulus without changing the original design.

Compared with conventional SDR, there are several unique features for cage-tuned SDR. First, the exponential length dependence of the rate of the SDR allows only for a rather coarse change as the toehold length can only be changed one base at a time. Addition of cage **1** with the correct concentration enables fine-tuning of the kinetics by adjusting the cage concentration without changing the original design. Second, the cage-based modulation is controllable with additional external parameters. Our metal−organic cage is formed through self-assembly of metal ions and organic ligands with adjustable stability. For example, the cage can be disassembled by heat or chelating agents, thus enabling control over SDR. Third, targeted modulation of one specific SDR is possible by using the cage. As shown in Figure 2, the negative charge of the DNA side chain in the toehold domain is vital for the cage binding. By making the target toehold more negatively charged or by making other toeholds neutral, we can realize targeted modulation of the desired SDR in the future. Finally, the cage may also be used to tune SDR in different nanosystems, providing an external mechanism to precise control. Given the significance of toehold-mediated DNA SDR across numerous fields, including nanotechnology, molecular computing, and biosensing, this method and other new applications of metal−organic cages to mediate DNA interactions show great promise.

## ■ ASSOCIATED CONTENT

### Supporting Information

The Supporting Information is available free of charge at https://pubs.acs.org/doi/10.1021/acs.nanolett.0c04125.

Details of DNA sequences, synthesis of cage, supplementary data (PDF)

## ■ AUTHOR INFORMATION

### Corresponding Authors

**Ulrich F. Keyser** − *Cavendish Laboratory, University of Cambridge, Cambridge CB3 0HE, United Kingdom;*



https://dx.doi.org/10.1021/acs.nanolett.0c04125
*Nano Lett.* 2021, 21, 1368−1374

orcid.org/0000-0003-3188-5414; Email: ufk20@cam.ac.uk

**Jonathan R. Nitschke** − *Department of Chemistry, University of Cambridge, Cambridge CB2 1EW, United Kingdom;* orcid.org/0000-0002-4060-5122; Email: jrn34@cam.ac.uk

### Authors

**Jinbo Zhu** − *Cavendish Laboratory, University of Cambridge, Cambridge CB3 0HE, United Kingdom;* orcid.org/0000-0003-4935-825X

**Filip Bošković** − *Cavendish Laboratory, University of Cambridge, Cambridge CB3 0HE, United Kingdom;* orcid.org/0000-0001-7663-2408

**Bao-Nguyen T. Nguyen** − *Department of Chemistry, University of Cambridge, Cambridge CB2 1EW, United Kingdom*

Complete contact information is available at: https://pubs.acs.org/10.1021/acs.nanolett.0c04125

### Notes

The authors declare no competing financial interest.

## ■ ACKNOWLEDGMENTS

J.Z., J.R.N., and U.F.K. thank the support from the UK Engineering and Physical Sciences Research Council (EPSRC, EP/M008258/1). J.Z. and U.F.K. thank the support from the ERC Consolidator Grant (Designerpores No. 647144). F.B. acknowledges funding from George and Lilian Schiff Foundation Studentship, the Winton Programme for the Physics of Sustainability, and St. John's Benefactors' Scholarship. We thank Diana Sobota for the suggestions on the manuscript.

## ■ REFERENCES

(1) Simmel, F. C.; Yurke, B.; Singh, H. R. Principles and applications of nucleic acid strand displacement reactions. *Chem. Rev.* **2019**, *119*, 6326−6369.

(2) Yurke, B.; Turberfield, A. J.; Mills, A. P.; Simmel, F. C.; Neumann, J. L. A DNA-fuelled molecular machine made of DNA. *Nature* **2000**, *406*, 605−608.

(3) Qian, L.; Winfree, E.; Bruck, J. Neural network computation with DNA strand displacement cascades. *Nature* **2011**, *475*, 368−372.

(4) Zhu, J.; Zhang, L.; Li, T.; Dong, S.; Wang, E. Enzyme-free unlabeled DNA logic circuits based on toehold-mediated strand displacement and split G-quadruplex enhanced fluorescence. *Adv. Mater.* **2013**, *25*, 2440−2444.

(5) Qian, L.; Winfree, E. Scaling up digital circuit computation with DNA strand displacement cascades. *Science* **2011**, *332*, 1196−1201.

(6) Tang, W.; Zhong, W.; Tan, Y.; Wang, G. A.; Li, F.; Liu, Y. DNA strand displacement reaction: a powerful tool for discriminating single nucleotide variants. *Topics Curr. Chem.* **2020**, *378*, 10.

(7) Li, B.; Ellington, A. D.; Chen, X. Rational, modular adaptation of enzyme-free DNA circuits to multiple detection methods. *Nucleic Acids Res.* **2011**, *39*, No. e110-e110.

(8) Xuan, F.; Hsing, I. M. Triggering hairpin-free chain-branching growth of fluorescent DNA dendrimers for nonlinear hybridization chain reaction. *J. Am. Chem. Soc.* **2014**, *136*, 9810−9813.

(9) Muscat, R. A.; Bath, J.; Turberfield, A. J. A programmable molecular robot. *Nano Lett.* **2011**, *11*, 982−987.

(10) Thubagere, A. J.; Li, W.; Johnson, R. F.; Chen, Z.; Doroudi, S.; Lee, Y. L.; Izatt, G.; Wittman, S.; Srinivas, N.; Woods, D.; Winfree, E.; Qian, L. A cargo-sorting DNA robot. *Science* **2017**, *357*, No. eaan6558.

(11) Bath, J.; Green, S. J.; Allen, K. E.; Turberfield, A. J. Mechanism for a directional, processive, and reversible DNA motor. *Small* **2009**, *5*, 1513−1516.

(12) Kaufhold, W. T.; Brady, R. A.; Tuffnell, J. M.; Cicuta, P.; Di Michele, L. Membrane scaffolds enhance the responsiveness and stability of DNA-based sensing circuits. *Bioconjugate Chem.* **2019**, *30*, 1850−1859.

(13) Andersen, E. S.; Dong, M.; Nielsen, M. M.; Jahn, K.; Subramani, R.; Mamdouh, W.; Golas, M. M.; Sander, B.; Stark, H.; Oliveira, C. L. P.; Pedersen, J. S.; Birkedal, V.; Besenbacher, F.; Gothelf, K. V.; Kjems, J. Self-assembly of a nanoscale DNA box with a controllable lid. *Nature* **2009**, *459*, 73−76.

(14) Bae, W.; Kocabey, S.; Liedl, T. DNA nanostructures in vitro, in vivo and on membranes. *Nano Today* **2019**, *26*, 98−107.

(15) Platnich, C. M.; Hariri, A. A.; Rahbani, J. F.; Gordon, J. B.; Sleiman, H. F.; Cosa, G. Kinetics of strand displacement and hybridization on wireframe DNA nanostructures: dissecting the roles of size, morphology, and rigidity. *ACS Nano* **2018**, *12*, 12836−12846.

(16) Cangialosi, A.; Yoon, C.; Liu, J.; Huang, Q.; Guo, J.; Nguyen, T. D.; Gracias, D. H.; Schulman, R. DNA sequence-directed shape change of photopatterned hydrogels via high-degree swelling. *Science* **2017**, *357*, 1126−1130.

(17) Kuzyk, A.; Schreiber, R.; Zhang, H.; Govorov, A. O.; Liedl, T.; Liu, N. Reconfigurable 3D plasmonic metamolecules. *Nat. Mater.* **2014**, *13*, 862−866.

(18) Zhang, Y.; McMullen, A.; Pontani, L. L.; He, X.; Sha, R.; Seeman, N. C.; Brujic, J.; Chaikin, P. M. Sequential self-assembly of DNA functionalized droplets. *Nat. Commun.* **2017**, *8*, 21.

(19) Groves, B.; Chen, Y. J.; Zurla, C.; Pochekailov, S.; Kirschman, J. L.; Santangelo, P. J.; Seelig, G. Computing in mammalian cells with nucleic acid strand exchange. *Nat. Nanotechnol.* **2016**, *11*, 287−294.

(20) Zhang, D. Y.; Winfree, E. Control of DNA strand displacement kinetics using toehold exchange. *J. Am. Chem. Soc.* **2009**, *131*, 17303−17314.

(21) Genot, A. J.; Zhang, D. Y.; Bath, J.; Turberfield, A. J. Remote toehold: a mechanism for flexible control of DNA hybridization kinetics. *J. Am. Chem. Soc.* **2011**, *133*, 2177−2182.

(22) Yang, X.; Tang, Y.; Traynor, S. M.; Li, F. Regulation of DNA strand displacement using an allosteric DNA toehold. *J. Am. Chem. Soc.* **2016**, *138*, 14076−14082.

(23) Dalgarno, S. J.; Power, N. P.; Atwood, J. L. Metallo-supramolecular capsules. *Coord. Chem. Rev.* **2008**, *252*, 825−841.

(24) Tranchemontagne, D. J.; Ni, Z.; O'Keeffe, M.; Yaghi, O. M. Reticular chemistry of metal-organic polyhedra. *Angew. Chem., Int. Ed.* **2008**, *47*, 5136−5147.

(25) Jones, L. O.; Mosquera, M. A.; Fu, B.; Schatz, G. C.; Ratner, M. A.; Marks, T. J. Germanium fluoride nanocages as optically transparent n-type materials and their endohedral metallofullerene derivatives. *J. Am. Chem. Soc.* **2019**, *141*, 1672−1684.

(26) Evariste, S.; Khalil, A. M.; Moussa, M. E.; Chan, A. K.-W.; Hong, E. Y.-H.; Wong, H. L.; Le Guennic, B.; Calvez, G.; Costuas, K.; Yam, V. W. W.; Lescop, C. Adaptive coordination-driven supramolecular syntheses toward new polymetallic Cu(I) luminescent assemblies. *J. Am. Chem. Soc.* **2018**, *140*, 12521−12526.

(27) Brown, C. J.; Toste, F. D.; Bergman, R. G.; Raymond, K. N. Supramolecular catalysis in metal-ligand cluster hosts. *Chem. Rev.* **2015**, *115*, 3012−3035.

(28) Grommet, A. B.; Nitschke, J. R. Directed phase transfer of an FeII4L4 cage and encapsulated cargo. *J. Am. Chem. Soc.* **2017**, *139*, 2176−2179.

(29) Cui, Y.; Chen, Z. M.; Jiang, X. F.; Tong, J.; Yu, S. Y. Self-assembly and anion sensing of metal-organic [M6L2] cages from fluorescent triphenylamine tri-pyrazoles with dipalladium(ii, ii) corners. *Dalton Trans.* **2017**, *46*, 5801−5805.

(30) Fiedler, D.; Bergman, R. G.; Raymond, K. N. Stabilization of reactive organometallic intermediates inside a self-assembled nanoscale host. *Angew. Chem., Int. Ed.* **2006**, *45*, 745−748.

(31) Ahmad, N.; Younus, H. A.; Chughtai, A. H.; Verpoort, F. Metal-organic molecular cages: applications of biochemical implications. *Chem. Soc. Rev.* **2015**, *44*, 9−25.
(32) Mosquera, J.; Henriksen-Lacey, M.; García, I.; Martínez-Calvo, M.; Rodríguez, J.; Mascareñas, J. L.; Liz-Marzán, L. M. Cellular uptake of gold nanoparticles triggered by host-guest interactions. *J. Am. Chem. Soc.* **2018**, *140*, 4469−4472.
(33) Fernández-Caro, H.; Lostalé-Seijo, I.; Martínez-Calvo, M.; Mosquera, J.; Mascareñas, J. L.; Montenegro, J. Supramolecular caging for cytosolic delivery of anionic probes. *Chem. Sci.* **2019**, *10*, 8930−8938.
(34) Mosquera, J.; García, I.; Henriksen-Lacey, M.; Martínez-Calvo, M.; Dhanjani, M.; Mascareñas, J. L.; Liz-Marzán, L. M. Reversible control of protein corona formation on gold nanoparticles using host-guest interactions. *ACS Nano* **2020**, *14*, 5382−5391.
(35) Pöthig, A.; Casini, A. Recent developments of supramolecular metal-based structures for applications in cancer therapy and imaging. *Theranostics* **2019**, *9*, 3150−3169.
(36) Yu, G.; Yu, S.; Saha, M. L.; Zhou, J.; Cook, T. R.; Yung, B. C.; Chen, J.; Mao, Z.; Zhang, F.; Zhou, Z.; Liu, Y.; Shao, L.; Wang, S.; Gao, C.; Huang, F.; Stang, P. J.; Chen, X. A discrete organoplatinum-(II) metallacage as a multimodality theranostic platform for cancer photochemotherapy. *Nat. Commun.* **2018**, *9*, 4335.
(37) Drozdz, W.; Walczak, A.; Bessin, Y.; Gervais, V.; Cao, X.-Y.; Lehn, J.-M.; Ulrich, S.; Stefankiewicz, A. R. Multivalent metallosupramolecular assemblies as effective DNA binding agents. *Chem. - Eur. J.* **2018**, *24*, 10802−10811.
(38) Zhu, J.; Haynes, C. J. E.; Kieffer, M.; Greenfield, J. L.; Greenhalgh, R. D.; Nitschke, J. R.; Keyser, U. F. FeII4L4 tetrahedron binds to nonpaired DNA bases. *J. Am. Chem. Soc.* **2019**, *141*, 11358−11362.
(39) Bilbeisi, R. A.; Clegg, J. K.; Elgrishi, N.; Hatten, X. d.; Devillard, M.; Breiner, B.; Mal, P.; Nitschke, J. R. Subcomponent self-assembly and guest-binding properties of face-capped Fe4L48+ capsules. *J. Am. Chem. Soc.* **2012**, *134*, 5110−5119.
(40) Roll, C.; Ketterlé, C.; Faibis, V.; Fazakerley, G. V.; Boulard, Y. Conformations of nicked and gapped DNA structures by NMR and molecular dynamic simulations in water. *Biochemistry* **1998**, *37*, 4059−4070.
(41) Nazarenko, I.; Pires, R.; Lowe, B.; Obaidy, M.; Rashtchian, A. Effect of primary and secondary structure of oligodeoxyribonucleotides on the fluorescent properties of conjugated dyes. *Nucleic Acids Res.* **2002**, *30*, 2089−2195.
(42) Srinivas, N.; Ouldridge, T. E.; Šulc, P.; Schaeffer, J. M.; Yurke, B.; Louis, A. A.; Doye, J. P. K.; Winfree, E. On the biophysics and kinetics of toehold-mediated DNA strand displacement. *Nucleic Acids Res.* **2013**, *41*, 10641−10658.


https://dx.doi.org/10.1021/acs.nanolett.0c04125
*Nano Lett.* 2021, 21, 1368−1374